AGSO Journal of Australian Geology & Geophysics, 15 (3), 297–312

Early, methane-rich fluids and their role in Archaean gold mineralisation at the Sand King and Missouri deposits, Eastern Goldfields Province, Western Australia

T.P. Mernagh[1] & W.K. Witt[2]

The Sand King and Missouri lode gold deposits in the Siberia district of the Eastern Goldfields Province are situated within an amphibolite-facies metamorphic aureole in deformed greenstones flanking a monzogranitic batholith, which crops out less than 1 km to the west. The Missouri deposit was mined from 1899 to 1912 and again in 1987–1988 and produced approximately 921 kg of gold. The Sand King mine has produced about 4000 kg of gold since 1980. Gold occurs in the margins of the quartz (–biotite–pyrite) veins and in the alteration assemblage adjacent to the vein systems. Fluid inclusions in quartz and carbonate veins from both deposits have been studied by microthermometry and Raman spectrometry and have been classified into six types according to their chemical composition. The vapour phase of Type I inclusions contains pure or nearly pure CH_4 and the liquid-rich inclusions which appear least likely to have leaked contain up to 5 mole% CH_4 and 95 mole% H_2O. Rare Type II inclusions are multiphase and contain approximately equal amounts of CO_2 and CH_4 in the vapour phase. They may also contain up to four solid phases, of which muscovite and carbonate have been identified by Raman spectroscopy. Type III inclusions may also contain a muscovite daughter crystal, but have highly variable vapour contents and CO_2/CH_4 ratios. Type IV inclusions are CO_2-rich and may be either monophase or occur as liquid + vapour CO_2 ($\pm H_2O$) at room temperature. Type V inclusions are aqueous inclusions with an average salinity of 5.8 equiv. wt.% NaCl, and Type VI are high salinity inclusions (~27 equiv. wt.% $CaCl_2$) that may contain halite and two other unidentified solids.

The textural evidence suggests that Type I inclusions were trapped in the early phases of mineralisation at both the Sand King and Missouri deposits, around 500 to 600°C and 3–4 kbar. The fluid inclusions also provide evidence for mixing of the CH_4-rich Type I fluid with a CO_2-rich fluid. The latter may be related to a pervasive synmetamorphic fluid responsible for regional carbonation of the deformed metavolcanic rocks. Heterogeneous trapping is thought to be largely responsible for the variation in vapour content and CO_2/CH_4 ratio in inclusion Types II and III. The presence of muscovite as a daughter mineral in Types II and III links them to a potassic alteration event which is evident at both deposits. Type IV inclusions contain little or no detectable CH_4, which indicates that CO_2-rich fluids continued to circulate after most of the CH_4 and H_2 in the system had been consumed. The aqueous Types V and VI inclusions are thought to represent, respectively, late influx of meteoric waters and connate brines.

The early methane-bearing fluids indicate low fO_2 conditions, which may have been generated during the serpentinisation of nearby ultramafic rocks or, alternatively, could have been derived from a deep source in the crust or lower mantle. The addition of methane to the CO_2-rich ore-bearing fluid by fluid mixing greatly increases the field of fluid immiscibility over that of the conventional CO_2–H_2O–NaCl system. Thus, the fluid unmixes over a larger range of P–T conditions when methane is present and the sulphur content of the fluid diminishes as H_2S is strongly partitioned in the vapour phase during subsequent phase separation. These effects destabilise the auriferous sulphide ligands in solution and, hence, trigger gold precipitation. They may thus be important factors controlling gold precipitation under greenschist and amphibolite facies conditions.

Introduction

In recent years, it has become evident that Archaean lode-style gold deposits have formed over a wide temperature range and metamorphic grades from prehnite-pumpellyite to granulite facies. These observations have led to the suggestion of a continuum of gold deposit styles from shallow to deep crustal levels (Colvine et al. 1988; Foster 1989; Groves et al. 1992). Fluid inclusion and thermodynamic studies have documented a low-salinity H_2O–CO_2 fluid in many deposits hosted by greenschist-facies rocks (Smith et al. 1984; Robert & Kelly 1987; Ho et al. 1990), but data from higher grade rocks are relatively sparse. This paper presents the results of microthermometric and Raman microprobe analyses of fluid inclusions from amphibolite-facies-hosted deposits at Missouri and Sand King, in the Siberia district of the Eastern Goldfields Province, Western Australia. We have used these and other geological data to interpret the P–T–X evolution of the fluids from these two deposits and, in particular, present evidence for the existence of early methane-rich fluids.

Methane-bearing inclusions have been reported from a number of Archaean gold deposits of various metamorphic grades. $CO_2 \pm CH_4$ inclusions with rare thin water rims have been reported from the Wiluna deposit (Hagemann et al. 1992), which is a high crustal level deposit in prehnite-pumpellyite facies metamorphic terrain. Deposits in greenschist terrains which contain methane-bearing fluid inclusions include Lancefield, the Golden Mile, Mount Charlotte, Water Tank Hill and Granny Smith in the Yilgarn Block, Western Australia (Ho et al. 1990; Hagemann & Ridley 1993) and the McIntyre-Hollinger (Smith et al. 1984) and Sigma (Robert & Kelly 1987) mines in the Abitibi greenstone belt in Canada. Some very CH_4-rich ($X_{CH_4} \leq 0.8$) fluid inclusions have been observed in recent studies of the Corinthia-Hopes Hill, Marvel Loch, Three Mile Hill and Griffins Find deposits, which occur in amphibolite to granulite facies domains in the Yilgarn Block in Western Australia (Hagemann & Ridley 1993). It is also interesting to note that methane-bearing fluid inclusions and the widespread occurrence of graphite have been reported (Lapointe & Chown 1993) from the metamorphosed iron-formation of the Lac Lilos gold prospect in the Eastern Superior Province of the Canadian Shield. This prospect is in a granulite terrain and is thought to represent a deep-level expression of the crustal-scale mineralising systems documented for the late Archaean.

Regional geologic setting

The Sand King and Missouri deposits are in the Siberia district of the Eastern Goldfields Province (Fig. 1). The metavolcanic rocks in this district record four stages of deformation (Witt 1993a). The age of mineralised struc-

[1] Australian Geological Survey Organisation, GPO Box 378, Canberra ACT 2601, Australia.

[2] Geological Survey of Western Australia, 100 Plain Street, Perth, WA 6000, Australia.

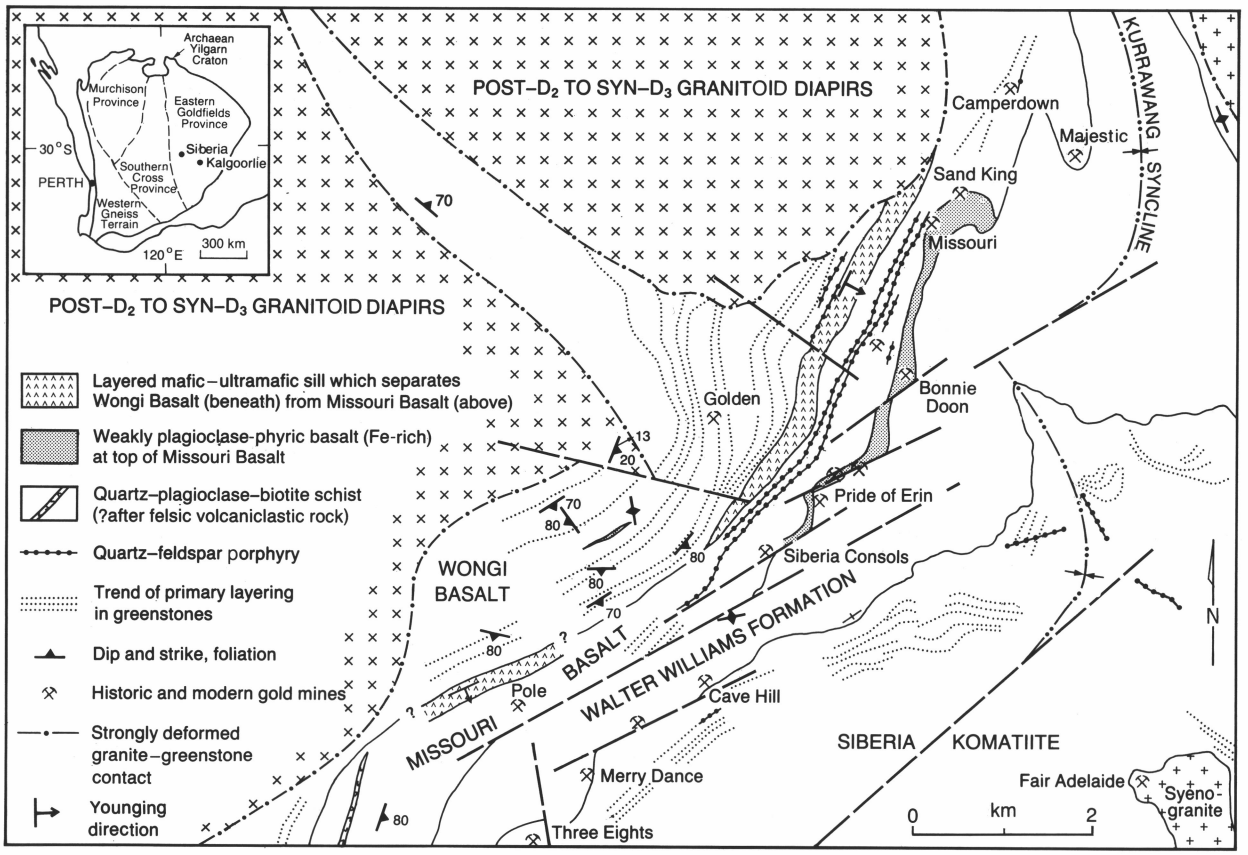

Figure 1. Geology and mines in the Siberia district, Eastern Goldfields Province.

tures is given by the timing of emplacement of the associated granitoid intrusion. The intrusion of monzogranitic diapirs to within 0.6 km of the deposits during D3 caused uplift and deformation of the metavolcanic rocks and generated the ductile to veined brittle-ductile shear zones which host the gold at Missouri and Sand King. Textural evidence from the mineralised structures and associated metasomatised host rock (Witt 1993a) indicates that auriferous fluids were introduced during this stage of deformation, and that high fluid pressures actively contributed to the formation of these structures.

Both deposits are hosted by fractionated Fe-rich tholeiitic basalt with small plagioclase phenocrysts. This pillowed basalt unit forms the uppermost part of the Missouri Basalt, which is locally interbedded with biotite–quartz–plagioclase schist with feldspar porphyroclasts. The Missouri Basalt is separated by a layered mafic/ultramafic sill from the underlying Wongi Basalt, and is overlain by olivine cumulates of the Walter Williams Formation and the Siberia Komatiite (Wyche & Witt 1992). The mafic rocks are strongly foliated in zones parallel to the monzogranite/greenstone contacts and a broad amphibolite-facies metamorphic aureole is developed over several kilometres adjacent to the contact. Small quartz–feldspar porphyry intrusions are generally conformable with primary layering in the greenstones and may be genetically related to late monzogranite intrusions (Witt 1992). An undeformed 080°-trending dolerite dyke south of the Missouri deposit forms part of the Proterozoic Widgiemooltha Dyke Suite (Myers 1990).

Most epigenetic lode gold deposits in the Eastern Goldfields Province with associated sericite–ankerite alteration are interpreted to have formed at 250–350°C and 1.5–2.5 kbar (Groves 1993). Deposits of this type include those along strike from the Siberia deposits (e.g. Ora Banda, Grants Patch, and Mount Pleasant), which formed more or less contemporaneously with Sand King and Missouri, during the final stages of regional deformation (Witt 1993a). Sand King and Missouri occur 3–5 km stratigraphically below these typical 'epigenetic' deposits, and at slightly deeper structural levels. Therefore, the Sand King and Missouri deposits are estimated to have formed at approximately 3–4 kbar. Biotite-dominant alteration assemblages at Siberia record temperatures between 440 and 600°C (Witt 1991). The relatively high alteration temperatures are considered to reflect proximity to the adjacent synmetamorphic monzogranite intrusions as well as deeper structural levels. The available geochronological data indicate that most granitoids were emplaced by the time of peak metamorphism at about 2.66 Ga, but that gold mineralisation did not occur until 2.63 Ga (McNaughton et al. 1993).

A prolonged period of post-cratonisation weathering has led to the development of a thick laterite profile, typically consisting of ferruginous, mottled and saprolite zones (Smith 1983), in parts of the Siberia district. Although the modern open pits at Missouri and Sand King have won gold from unweathered Archaean rocks, much of the historic mining in the Siberia district exploited supergene gold in the laterite profile.

Missouri

The Missouri deposit (Fig. 2) produced 20.8 kg of gold between 1899 and 1912 in workings to a depth of

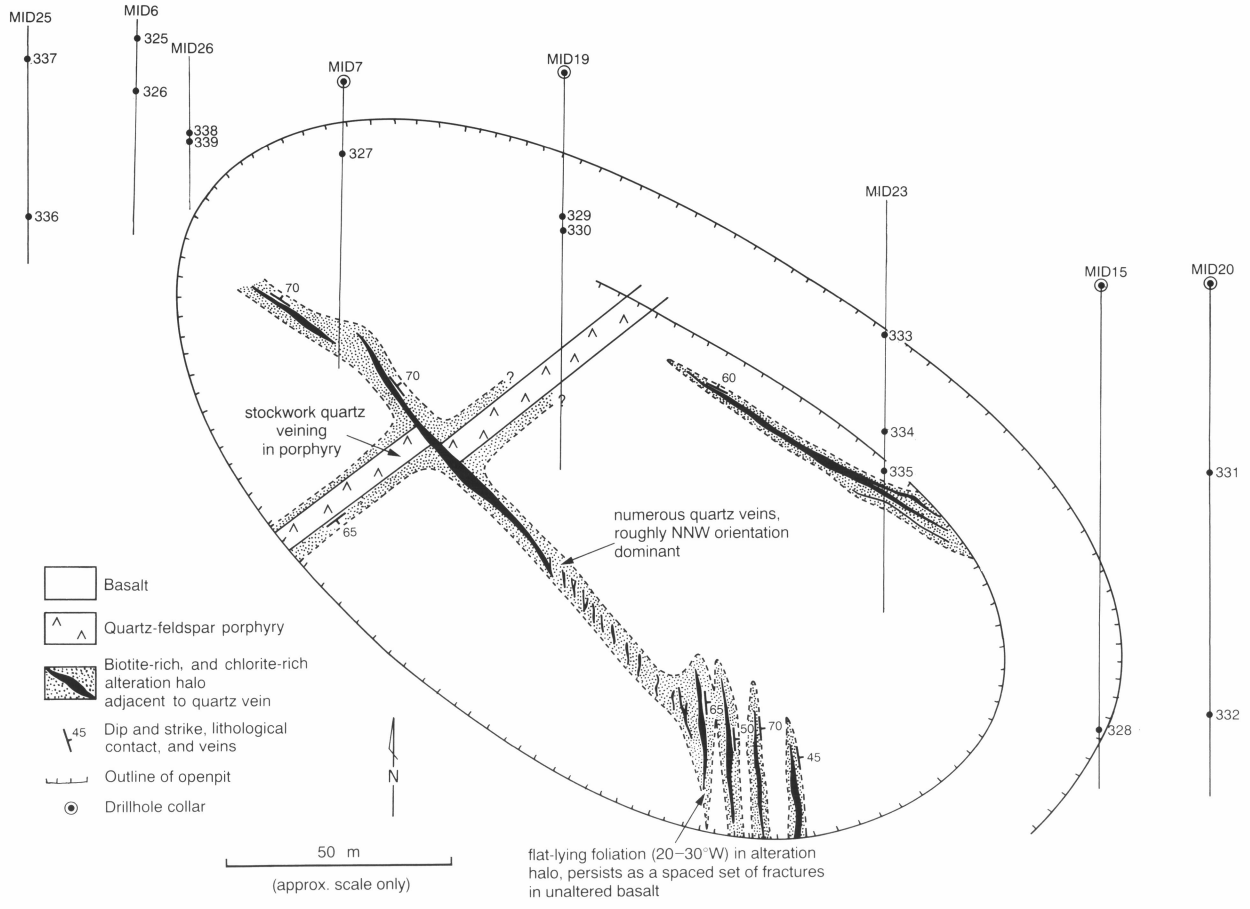

Figure 2. Geological plan of the Missouri open pit, showing the position of drill-holes and samples projected to the surface. Most drill-holes are inclined ~60° S.

approximately 100 m (Montgomery 1909). Further open pit mining during 1987 and 1988 produced approximately 900 kg Au (Witt 1993b). The mineralisation occurs in a 0.5–2 m wide, northwest-trending zone of quartz veins with minor ductile deformation and hydrothermal alteration in the adjacent host rocks. The mineralised zone dips approximately 70° northeast, but breaks up into several en echelon veins at the southeastern end of the open pit. These en echelon veins strike 345–355° and dip 45–70° northeast, consistent with dextral displacement and northeast-side-up movement.

Quartz(–plagioclase)–biotite–carbonate–pyrite alteration assemblages are developed adjacent to quartz veins. Oriented biotite grains locally define a weak shear fabric parallel to the quartz veins. Pyrite occurs as coarse (≤2 mm), idioblastic grains with small biotite-rich pressure shadows. The biotite-rich alteration assemblage is enveloped by a mildly chloritic outer alteration halo of a similar width, and minor late chlorite overprints biotite and the shear fabric in the inner alteration zone.

Sand King

The Sand King deposit (Fig. 3) has produced about 4000 kg of gold since 1980, but contains an underground resource, as yet unmined, of approximately 4500 kg of gold (Witt 1993b). Quartz–feldspar porphyry dykes, varying in width from 0.5 to 5 m, intrude the basalt and are flanked by barren, sulphide-absent biotitic alteration (Hill & Bird 1990). Sinistral north–south faults, 1 to 6 m wide, offset some of the porphyry dykes and are cross-cut by the mineralised vein system. A northeast-trending and northwest-dipping fault (not shown in Fig. 3) along the southern wall of the open pit appears to have controlled formation of the mineralised veins (Hill & Bird 1990).

The ore is hosted by zones of quartz (–biotite–pyrite) veins and breccias, which trend 090–060° and dip 70–80°N. Individual quartz veins vary from 1 mm to >5 m wide and the en echelon arrangement of the quartz veins defines a broad 050° trend. Best gold grades (up to 11 g/t) occur in the basaltic rocks adjacent to the porphyry intrusions and at intersections of the mineralised zone with north–south faults. Gold occurs at the margins of the quartz(–biotite–pyrite) veins and in the 0.5–2 m wide biotite–plagioclase–pyrite(–pyrrhotite) alteration assemblage adjacent to the vein systems. Gold occurs mainly as inclusions and in fractures within pyrite. Other sulphides (galena, chalcopyrite, sphalerite) and tellurides (hessite, petzite, altaite, tellurobismuthite, melonite), freibergite, and scheelite occur in minor quantities (Hill & Bird 1990). Minor fuchsite occurs in some quartz veins, and quartz–amphibole veins with amphibole-rich alteration selvages occur locally. Grossularite garnet has been observed in veins and alteration selvages towards the western end of the system, which lies close to the contact with one of the monzogranite plutons.

Analytical procedures

All analytical work was carried out at the Australian

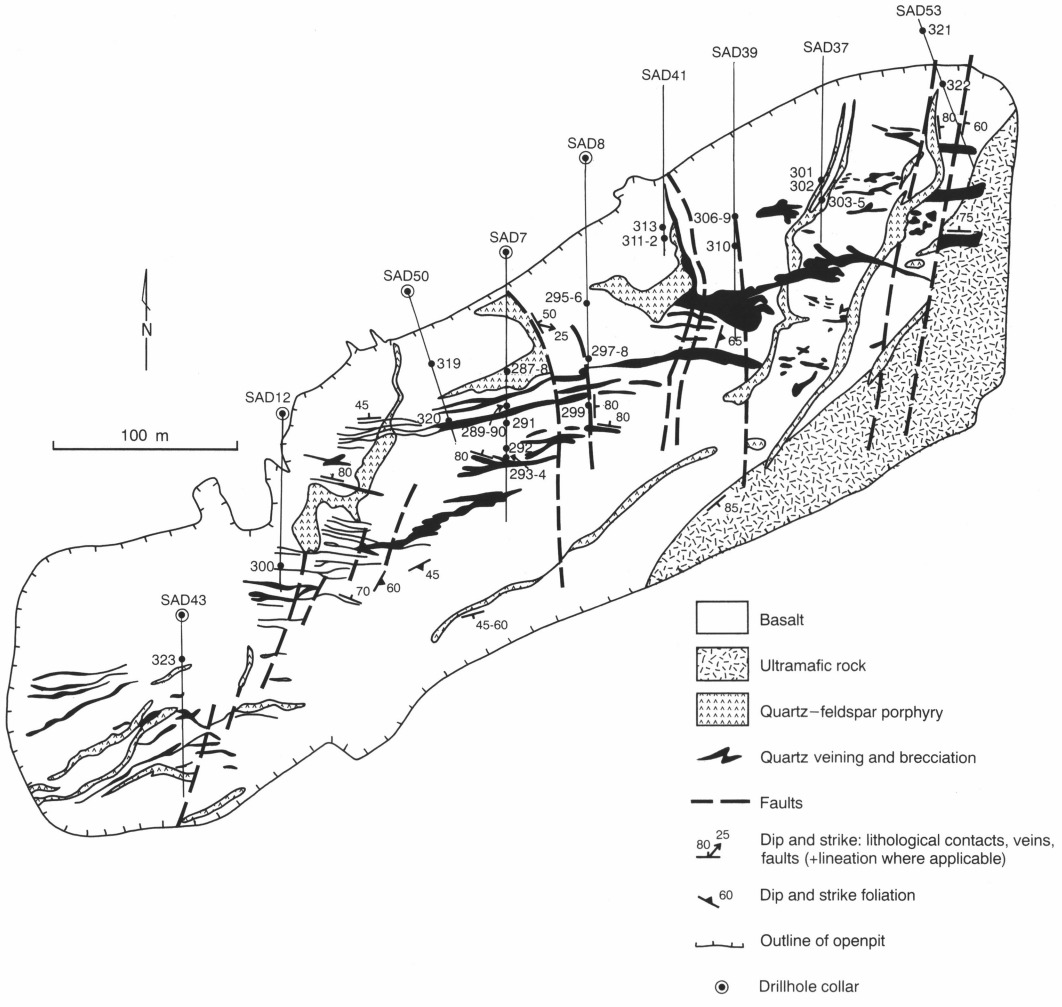

Figure 3. Geological plan of the Sand King open pit mine (after Bird & Pilapil 1988), showing the position of drill-holes and samples projected to the surface. Most drill-holes are inclined ~60° S.

Geological Survey Organisation's fluid-inclusion laboratories. Thermometric data were obtained from a Fluid Inc.-adapted USGS gas-flow system (Woods et al. 1981; Shepherd et al. 1985) and also from a Linkam heating–freezing stage (Shepherd et al. 1985) fitted to the microscope stage of the Raman microprobe. Both systems were calibrated with the same set of synthetic fluid inclusions (manufactured by Synflinc Ltd). Freezing measurements are estimated to be accurate to ± 0.5°C, while homogenisation temperatures have an estimated accuracy of ± 5°C.

Raman microprobe analyses were obtained from a Microdil 28 spectrometer (Liu & Mernagh 1990), using 40 mW (at the sample) of 514.5 nm laser excitation from a Spectra Physics 2020 5W Ar^+ laser. Spectra were typically obtained after 10 accumulations with a 5 second integration time and an approximately 5 cm^{-1} spectral bandpass. The Raman spectra were calibrated using Ar^+ plasma and neon emission lines; wave numbers were measured from the position of the peak maximum and are accurate to ± 1 cm^{-1}. The ratios of gases in the vapour phase were calculated using the method described by Dubessy et al. (1989) and the following 'quantification factors' were calculated as outlined in Pasteris et al. (1988): CO_2 = 1.3; N_2 = 1.0; H_2S = 6.4; CH_4 = 7.6 and C_2H_6 = 13.0. Raman detection limits are dependent on instrumental sensitivity and the partial pressure of each gas, but are estimated to be about 0.15 MPa for CO_2, O_2, N_2 and 0.03 MPa for H_2S and CH_4 under the conditions of this study. The salinity of carbonic inclusions was determined from the Raman spectra of the aqueous phase, using the skewing parameter method of Mernagh & Wilde (1989), which allows salinities to be determined to within ± 2 equivalent weight per cent NaCl.

Nature and occurrence of fluid inclusions

Fluid inclusions were examined in 20 doubly polished sections of quartz (± carbonate) veins selected from 38 samples of drill core from the Sand King deposit and in 8 doubly polished sections chosen from 15 samples of drill core from Missouri. Drill holes from which samples were collected are projected onto near-surface pit geology in Figures 2 and 3.

Two types of quartz are distinguished in the mineralised veins. The first and apparently earliest type of quartz shows undulose extinction, indicating limited amounts of ductile deformation. This 'relic' quartz contains dense populations of dominantly vapour-rich fluid inclusions. The second type occurs as sub-grains, mainly around the margins of the larger 'relic' grains of quartz and near the margins of the veins with wall rock. This recrystallised quartz is relatively unstrained. Most pre-existing fluid

inclusions were probably degraded during dynamic recrystallisation (Wilkins & Barkas 1978) and this later generation of quartz is characterised by relatively few small inclusions (generally <5 μm) near grain boundaries, except for grains with inclusions trapped in late secondary fractures.

Short, discontinuous, healed fractures, typically outlined by vapour-rich fluid inclusions, are observed in both types of quartz. They are generally parallel or subparallel to the vein walls and may cut across grain boundaries. In some samples, a second set of healed fractures with generally smaller aqueous inclusions is observed to intersect the other fractures at approximately 90°. A series of late secondary aqueous inclusions forms relatively continuous, cross-cutting trails. The relationships described suggest alternating periods of brittle and ductile deformation in a dynamic tectonic environment (cf. Robert & Brown 1986), although the mineralised vein system formed in a predominantly brittle deformation regime (Witt 1993b).

The fluid inclusions have been classified according to their composition, determined by microthermometry and Raman microprobe analyses (Table 1).

Type I inclusions (CH_4–H_2O)

These inclusions have negative crystal to irregular shapes and contain CH_4 as the dominant constituent of the vapour phase. Sizes vary up to about 20 μm, but most are only a few micrometres across. Trace amounts of CO_2 (<5 mole%) were detected by Raman spectroscopy in a small number of vapour-rich inclusions from this group. Some inclusions contain between 50 and 90 volume per cent liquid water, but others appear to contain only methane at room temperature (Figs 4A and 5). The range of observed H_2O/CH_4 ratios could be accounted for by invoking post-entrapment changes (Hollister 1990; Bakker & Jansen 1990), resulting in the loss of H_2O via mechanisms similar to those proposed for CO_2 rich inclusions (see below).

The CH_4-rich phase in these inclusions homogenised to liquid or by critical behaviour at temperatures from –87.9 to –71.8°C (Fig. 6A). The majority of inclusions showed homogenisation temperatures for the CH_4-rich phase which were slightly above the critical temperature of CH_4 (–82.6°C), indicative of the presence of minor amounts of CO_2. However, the data of Donnelly & Katz (1954) indicate that X_{CO_2} lies in the range 0 to 0.05 and the CO_2/CH_4 ratio could be even lower as CH_4 is selectively partitioned into the clathrate phase (Ramboz et al. 1985; Seitz et al. 1987), which was present or assumed to be present in all Type I inclusions at the temperature of homogenisation of the carbonic phase.

The small size of the inclusions made it difficult to observe the final melting temperature of clathrate, but several water-rich inclusions showed clathrate melting between 14 and 16°C. The final melting point of ice could not be observed, owing to the presence of clathrate in the water-rich inclusions. However, the salinities determined from the Raman spectra of the aqueous phase were generally below 3 equivalent wt % NaCl in the liquid at room temperature (Fig. 7). Inclusions that were not monophase at room temperature generally decrepitated before total homogenisation, but a few were observed to

Table 1. Summary of fluid-inclusion properties.

Deposit	*Inclusion Type*	*Size Range (μm)*	*Volume % Vapour*	*Mole % CO_2 in the Vapour*	*Mole % CH_4 in the Vapour*	*Mole % H_2S in the Vapour*	*Tm [a] (°C)*	*Tm [b] Clath.*	*Salinity [c]*	*Th [d] Carb.*	*Th [e] Total*
Missouri	I	<1–20	10–50	n.d. [f]	100	n.d.			1.1±0.4	–82.7±0.5	338±48
Missouri	I	<1–20	90–100	<5	95–100	n.d.					
Sand King	I	<1–20	10–20	n.d.	100	n.d.		15±1	1.3±0.5	–79±4	
Missouri	II	<1–40	50–100	41–65	35–59	0.4	–64.5±1.3		14±7	–4.6±5.8	302±22
Sand King	II	<1–12	50–90	41–73	27–59	n.d.	–63.0±0.4	13±4	15±6		316±26
Missouri	III	<1–20	40–100	10–88	12–90	n.d.	–66.1±2.9	13±1	4.8±1.4	–3.2±6.2	305±18
Sand King	III	<1–22	20–100	5–94	6–95	n.d.	–65.3±2.2	11±3	3.5±0.9		286±44
Missouri	IV	<1–40	40–95	88–100	0–12	n.d.	–56.9±0.4	8.6±0.5	1.1±0.8	21±4	289±29
Sand King	IV	<1–20	40–95	79–100	0–21	n.d.	–59.1±1.8	11.5±1.4	1.9±0.9	10±10	323±27
Missouri	V	<1–50	5–10	n.d.	n.d.	n.d.	–2.4±1.2	n.d.	4.0±1.5	n.d.	191±25
Sand King	V	<1–20	5–10	n.d.	n.d.	n.d.	–3.3±1.2	n.d.	5.8±1.5	n.d.	132±56
Missouri	VI	<1–50	5–10	n.d.	n.d.	n.d.	–28.7±9.1	n.d.	28.4±10.8	n.d.	105±24
Sand King	VI	<1–30	5–10	n.d.	n.d.	n.d.	–30.9±8.5	n.d.	29.8±9.6	n.d.	85±23

[a] Melting temperature of solid CO_2 in Types I–IV and the melting temperature of ice in Types V–VI. The results are given as an average followed by the standard deviation.

[b] CO_2±CH_4 clathrate melting temperature (°C).

[c] Fluid salinity in equivalent weight per cent NaCl, determined by Raman spectroscopy.

[d] Homogenisation temperature (°C) of the carbonic (CH_4 or CO_2 or both) phase.

[e] Total homogenisation temperature of the fluid inclusion (°C).

[f] n.d. = not detected.

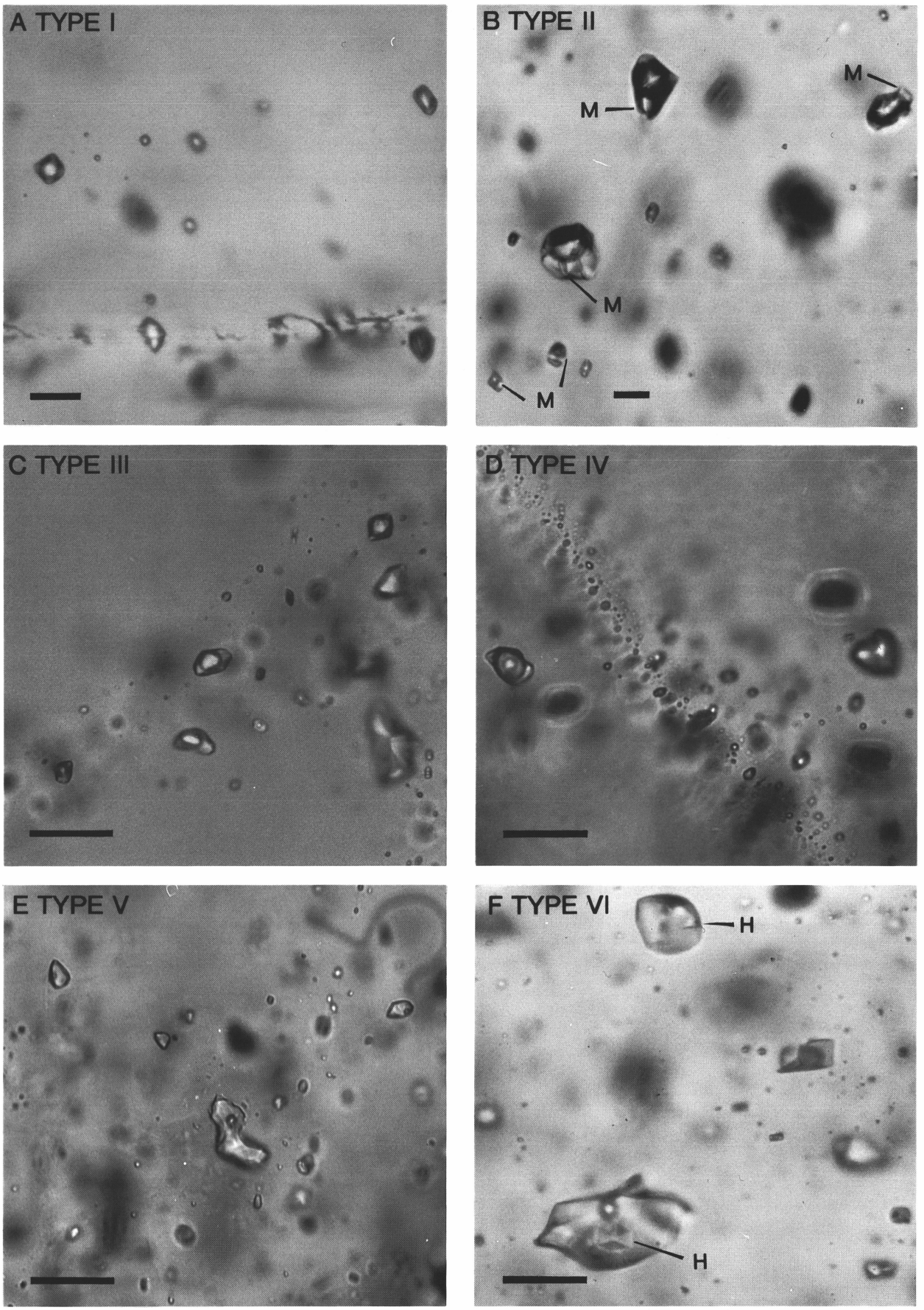
A TYPE I
B TYPE II
M
M
M
M
C TYPE III
D TYPE IV
E TYPE V
F TYPE VI
H
H

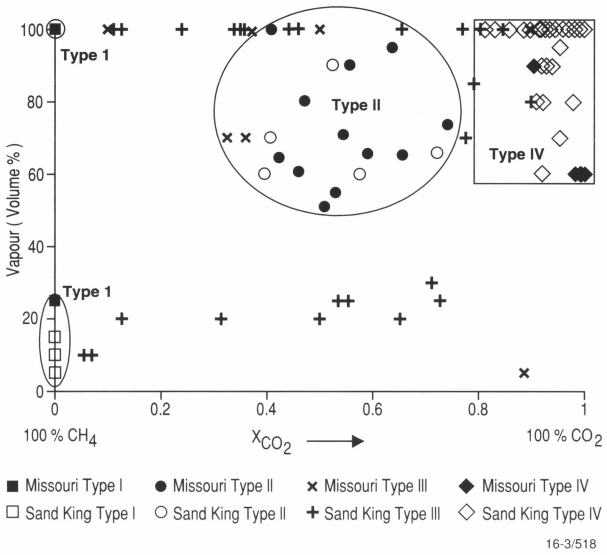

Figure 5. A plot of X_{CO_2} in the vapour phase versus vol.% vapour of inclusions for Raman microprobe analyses of inclusion Types I–IV.

homogenise over the temperature range 296–402°C with an average value of 338°C (Fig. 8A).

Type II (multiphase inclusions)

Multiphase inclusions containing up to four solid phases, an aqueous phase and greater than 50 vol. % vapour (Figs 4B and 5) have been classified as Type II. These inclusions are quite rare and have only been observed in 'relic' quartz surrounded by thin veins of sulphide or fuchsite (identified by Raman spectroscopy). Raman spectroscopy has also identified muscovite and carbonate in some of these inclusions. Sizes range from 40 μm or less and most have rounded or negative crystal morphology.

As shown in Figure 6B, melting of the carbonic phase in these inclusions occurs over a range from –68 to –60°C with a distinct mode near –64°C. Because CH_4 is strongly partitioned into the vapour phase and $Tm(CO_2)$ is only a function of the amount of CH_4 in the coexisting liquid phase, inclusions containing significant volumes of vapour are more CH_4-rich than indicated by $Tm(CO_2)$. Therefore, although the $Tm(CO_2)$ mode indicates 38 mole % CH_4 in the vapour phase (Swanenberg 1979), the Raman microprobe analyses (Fig. 5) indicate that the vapour phase in these inclusions contains an average of 49 mole % CO_2 and 51 mole % CH_4. Hydrogen sulphide (0.4 mole %) was also detected in the vapour phase of Type II inclusions from Missouri (Table 1) which were in relic quartz grains surrounded by thin veins of arsenopyrite.

Clathrate formation could only be observed in a few inclusions and their final melting temperatures ranged from 9 to 14°C, the majority melting between 13 and 14°C. The Raman spectra indicate that the aqueous phase has a salinity between 13 and 24.8 equiv. wt % NaCl (Fig. 7) with an average of 15 equiv. wt % NaCl. Although the salinity of these inclusions is considerably higher than any of the other carbonic inclusions, the aqueous phase appears to be undersaturated and thus these inclusions do not contain any solid chlorides, but only solid silicate and carbonate phases. These solid phases did not dissolve before decrepitation occurred at temperatures

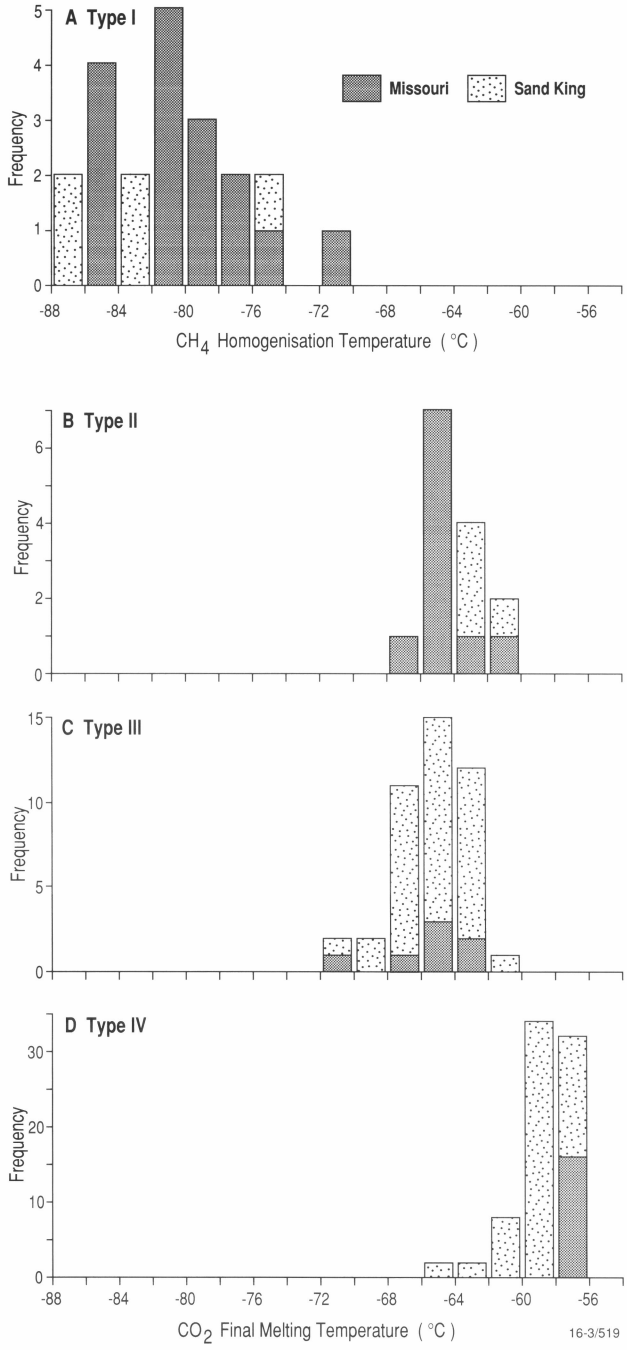

Figure 6. Homogenisation temperatures for the CH_4-rich vapour phase in (A) Type I inclusions, and final melting temperatures for CO_2 in (B) Type II, (C) Type III, and (D) Type IV inclusions.

Figure 4. Photomicrographs showing the nature of fluid inclusions at Missouri and Sand King. (A) Relatively isolated, vapour-rich Type I inclusions with only CH_4 detected in the vapour phase; (B) Multiphase, Type II inclusions in 'relic' quartz surrounded by fuchsite veins, 'M' denotes crystals of muscovite; (C) Type III inclusions containing both CO_2 and CH_4 in the vapour phase; (D) CO_2-rich Type IV inclusions, containing both liquid and vapour CO_2 cut by a trail of secondary aqueous inclusions; (E) low-salinity, Type V aqueous inclusions in quartz; (F) high-salinity, Type VI inclusions in calcite, some of which contain a halite daughter crystal, denoted by 'H'. Scale bars = 10 μm.

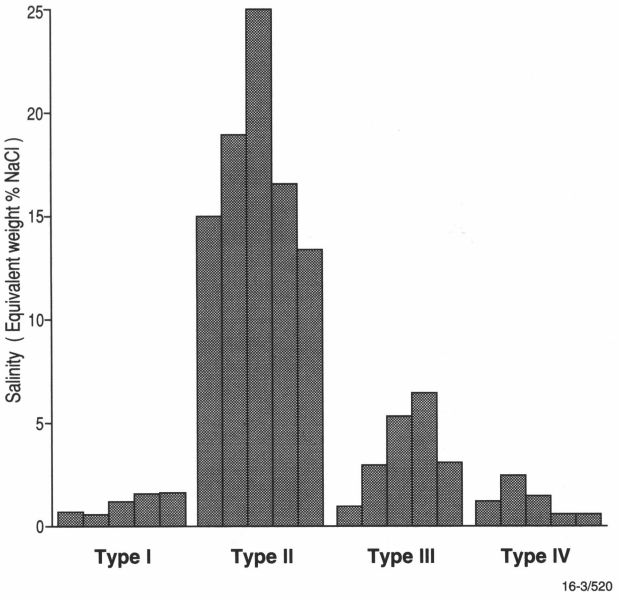

Figure 7. Salinity in equiv. wt % NaCl, as determined from Raman microprobe spectra of the aqueous phase of fluid inclusions, using the skewing parameter method described by Mernagh & Wilde (1989).

above 200°C. Homogenisation of aqueous and carbonic phases to a carbonic phase was observed in a few inclusions and covered the range from 287 to 335°C (Fig. 8B).

Type III inclusions (H_2O–CO_2–CH_4)

These inclusions consist of either one phase or two phases (an aqueous liquid + carbonic vapour) at room temperature (Fig. 4C). The carbonic phase contains both CO_2 and CH_4 and a few of these inclusions also contain a small daughter mineral, identified as muscovite by Raman spectroscopy. Individual fractures or clusters may have relatively constant or highly variable phase proportions.

Final CO_2 melting temperatures for Type III inclusions ranged from –71 to –61°C with an average value of –65.2°C (Fig. 6C), which indicates the presence of significant amounts of CH_4. The Raman microprobe analyses also confirmed a wide variation in $X(CO_2)$ in the vapour phase, which ranged from 0.86 to 0.09 (Fig. 5). The CO_2 content of the vapour phase is generally lower than that in Type II inclusions.

Homogenisation (l+v→v) of the carbonic phase was only observed in a few inclusions and varied from –8.7 to 7.6°C. These values are generally lower than those of Type II inclusions (see Fig. 6) and result from the higher CH_4 content of Type III inclusions. Clathrate melting was observed between 5.8 and 13.4°C with an average value of 11.2°C. The Raman spectra of the aqueous phase indicate that the salinity of the fluid is less than 7 equiv. wt % NaCl (Fig. 7). Most inclusions decrepitated before homogenisation, but a few were observed to homogenise into the carbonic phase between 220 and 338°C (Fig. 8C).

Type IV inclusions (CO_2–H_2O)

In many of these inclusions, only CO_2 is observed at room temperature, either as a single phase or as both liquid and vapour. Other CO_2-rich inclusions also contained an aqueous phase with the volumetric proportions of CO_2 ranging from 40 to 95%, but typically greater than 50% (Fig. 4D). Rare Type IV inclusions also contain a small carbonate daughter mineral. Inclusions up to a maximum size of about 40 μm have been observed and shapes vary from irregular to negative crystal forms.

Microthermometric studies show that solid CO_2 melts over the range –66 to –56.6°C with a mode around –58°C

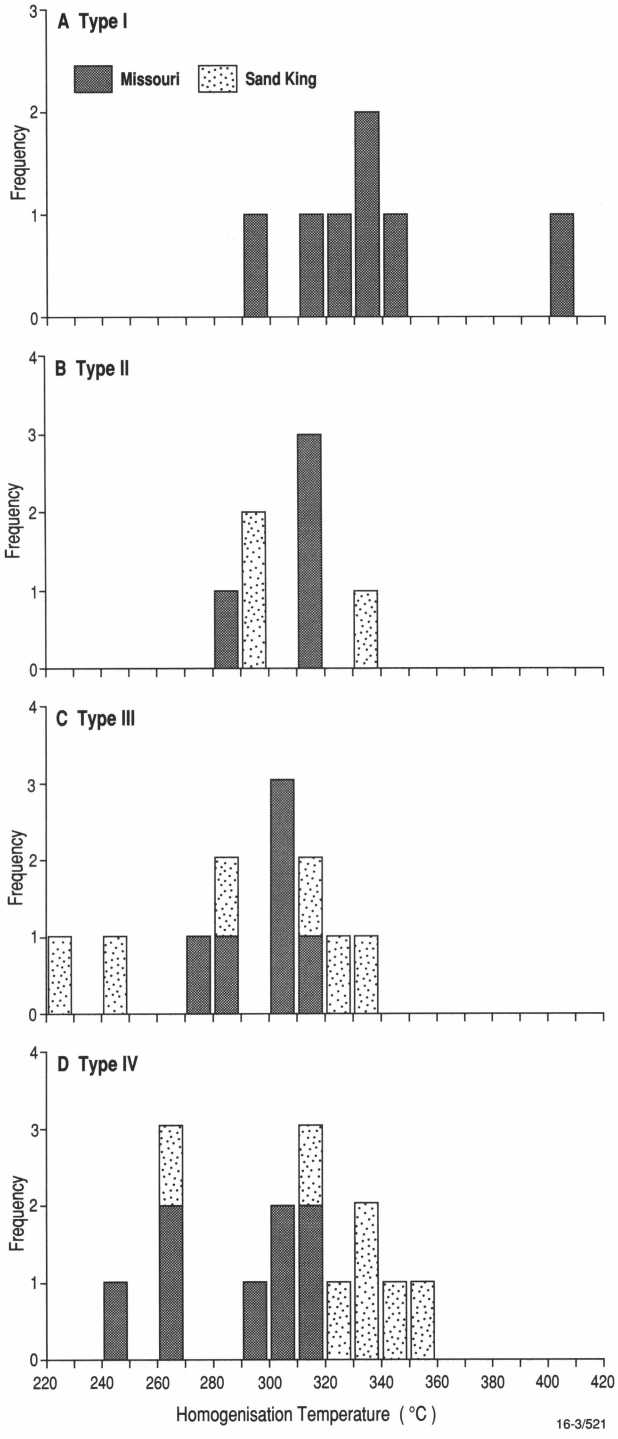

Figure 8. Total homogenisation temperatures for (A) Type I, (B) Type II, (C) Type III, and (D) Type IV inclusions. Note that the solids present in Types II and III inclusions generally did not dissolve before homogenisation of the liquid and vapour phases.

(Fig. 6D), and Raman microprobe analysis has shown that the depression in the melting point of CO_2 is caused by the presence of CH_4. The compositions of the vapour phase, as determined by Raman spectroscopy, are shown in Fig. 5. The CO_2 content of the vapour phase varies from 100 mole % down to 79 mole % with an average value of 93.8 mole % and the corresponding X_{CO2} of the inclusions varies from 0.10 to 0.85.

The CO_2 phases homogenise into the liquid phase at temperatures ranging from –8 to 31°C with a mode around 22°C. The spread of CO_2 homogenisation temperature indicates a wide range of densities (0.47–0.93) and it was noted that fluid inclusions from single grains or even single micro-fractures seldom had identical densities. Elsewhere, similar observations have been interpreted as resulting from heterogeneous trapping or as a result of volume changes after entrapment (cf. Robert & Kelly 1987; Santosh et al. 1991). The formation of clathrate was only observed in inclusions which exhibited an aqueous phase at room temperature. Clathrate melting temperatures ranged from 9 to 15°C, the majority melting around 9°C. However, a significant number of inclusions showed clathrate melting above 10°C (the invariant melting point of clathrate in the salt-free H_2O–CO_2 system) and hence, reflect the presence of minor CH_4 in these inclusions. Raman spectra indicated that the salinity was less than 3 equiv. wt % NaCl in these inclusions (Fig. 7).

Type IV inclusions which contained an observable aqueous phase typically decrepitated before total homogenisation, but a small number were observed to homogenise into the carbonic phase. Final homogenisation temperatures ranged from 240 to 360°C (Fig. 8D). Inclusions from Missouri generally had slightly lower homogenisation temperatures, with an average of 289°C, while inclusions from Sand King had an average of 323°C. These relatively high homogenisation temperatures further support the presence of a minor NaCl component in Type IV inclusions, since the critical curve for the salt-free H_2O–CO_2 system reaches a maximum of around 270°C at the inferred trapping pressures of 3–4kbar.

Type V (aqueous inclusions)

These are secondary, low-salinity, aqueous inclusions, some of which contain a vapour bubble of about 5 vol. % (Fig. 4E). The Raman microprobe did not detect any species in the vapour phase and, hence, H_2O is assumed to be the only volatile species. Individual inclusions are typically irregular, jagged or rounded, and vary in size up to approximately 50 μm. The irregularly shaped inclusions are generally flat-lying along the plane of the fracture and many show evidence of necking down. They represent relatively late fluids, as they generally outline healed fractures traversing the entire crystal, and have been observed to cross-cut trails of carbonic inclusions. Final melting temperatures of ice range from –5 to 0°C with a mode at –3.5°C, giving an average salinity of 5.8 equiv. wt % NaCl (Fig. 9A). Total homogenisation to the liquid phase occurred from 78 to 253°C, and there appears to be a bimodal distribution with modes around 100°C and 190°C (Fig. 10A), possibly representing the existence of two generations of low-salinity fluids.

Type VI (high-salinity aqueous inclusions)

Type VI inclusions typically contain 5–10 vol. % vapour and are relatively saline (Fig. 4F). They are rounded to irregular in shape and vary in size up to 50 μm. Most Type VI inclusions in quartz contained only vapour and brine. However, some inclusions in late calcite vein-fill contained a single halite crystal or, more rarely, up to three daughter minerals. The Raman microprobe could not detect any species in the vapour phase of Type VI inclusions and H_2O is assumed to be the only volatile species.

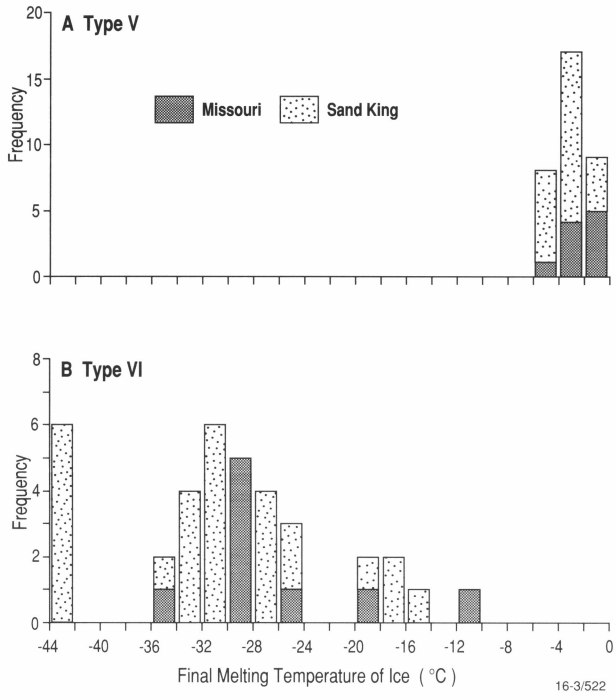

Figure 9. Final melting temperatures of ice in (A) Type V and (B) Type VI inclusions.

Inclusions in quartz have initial ice melting temperatures between –86 and –59°C and final ice melting temperatures

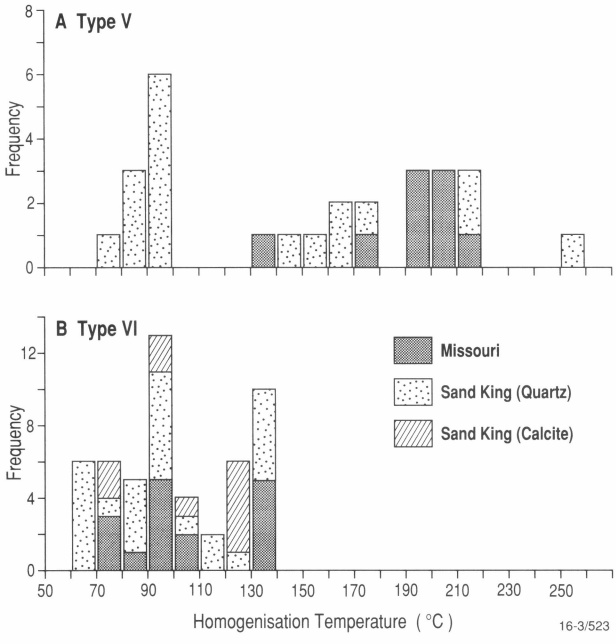

Figure 10. Total homogenisation temperatures for (A) Type V and (B) Type VI inclusions.

ranging from –44 to –11.5°C (Fig. 9B) with an average of –30.9°C or 26 equiv. wt % $CaCl_2$. The depression of the final ice melting temperature to as low as –44°C suggests that these fluids are $MgCl_2$-rich or $CaCl_2$-rich, as the eutectic melting temperature of $CaCl_2$ is –49.8°C (Crawford 1981). The very low eutectic melting temperatures observed in these inclusions may be due to the presence of metastable $MgCl_2$ x nH_2O or $CaCl_2$ x nH_2O complexes, which have reported first melting temperatures as low as –70°C (Davis et al. 1990). Homogenisation (l+v→l) temperatures range from 61 to 129°C (Fig. 10B), consistent with a late-stage influx of very saline fluids.

Inclusions in calcite have initial melting temperatures of –48 to –11°C, with an average of –32.2°C. This suggests that they may contain a brine similar to that in the quartz-hosted inclusions, but the presence of halite daughter crystals indicates a much higher Na^+ content in these fluids. Halite daughter crystals melted between 122 and 123°C, giving a salinity of 28.5 equiv. wt % NaCl (or 27 equiv. wt % $CaCl_2$). Total homogenisation to liquid occurred at temperatures between 76 and 139°C, which is again similar to those of Type VI inclusions in quartz.

Discussion

The CH_4-rich fluids

Methane-rich inclusions are rare, but their presence in early (relic) quartz and in quartz associated with biotite–carbonate–pyrite–wall rock alteration assemblages and their relatively high homogenisation temperatures suggest that they represent the earliest generation of fluid trapped in these deposits. Although the origin of the CH_4–H_2O fluid is not clear, possible sources for the fluid are evaluated below.

Methane-bearing fluids have been detected in a number of igneous (Konnerup-Madsen et al. 1985; Thomas et al. 1990; Larsen et al. 1992) and metamorphic environments (Hollister & Burrus 1976; Poutiainen 1990). Rumble & Hoering (1986) proposed that CH_4-rich fluids may form during greenschist to amphibolite facies grade metamorphism of graphitic pelites at 'low fO_2'. In fact, any rock plus fluid bulk composition that lies within the CH_4–H_2O–graphite field has an fO_2 very close to that defined by the quartz–fayalite–magnetite (QFM) buffer (Holloway 1984). Calculations by Ohmoto & Kerrick (1977) have shown that for fluid in equilibrium with graphite + pyrite + pyrrhotite at 2 kbar and 500°C, CH_4 becomes the dominant carbonic species at one log unit or more below the QFM buffer and at QFM–2, fluids on the graphite boundary consist of ~85 mol. % CH_4 and ~15 mol. % H_2O (Holloway 1981). However, there are few metapelitic rocks in the immediate mine area. The nearest metasedimentary rocks are several kilometres from the deposits and they have a quartzofeldspathic composition. Low fO_2 conditions favourable for the generation of methane could, however, occur during the serpentinisation of nearby ultramafic rocks (cf. Frost 1985).

Methane-bearing fluids may be stable to considerable depths within the Earth's crust, as a variety of heterogeneous equilibria (Buddington & Lindsley 1964; Eggler 1983; Haggerty & Tompkins 1985; Mattioli & Wood 1986) and intrinsic fO_2 measurements (Arculus & Delano 1981; Arculus et al. 1984) indicate that portions of the upper mantle and lower crust have values of fO_2 within ±2 log units of the QFM buffer. Therefore, the CH_4-bearing fluids could also be generated from a deep high-temperature source in the lower crust or mantle, where the fO_2 may be very close to QFM–2.

The vapour (CH_4)-rich Type I inclusions appear to result from post-entrapment modification of CH_4–H_2O inclusions rather than from phase separation. At high temperatures the CH_4–H_2O fluid will form a homogeneous supercritical fluid and this fluid will not unmix until the temperature falls below 325°C in the salt-free system (Holloway 1984). The addition of NaCl to the system will extend the two-phase region to higher temperatures (cf. Krader & Franck 1987); however, the Raman microprobe analyses indicate fairly low salinities (Fig. 7). Thus, it is unlikely that the CH_4–H_2O fluid would have unmixed at the temperatures recorded by mineralised alteration assemblages (i.e. >450°C).

The CO_2-bearing fluids

There is widespread evidence for the existence of a synmetamorphic, CO_2-bearing, aqueous fluid in all gold deposits of the Eastern Goldfields Province (Ho et al. 1990). This relatively oxidised fluid introduced massive amounts of carbonate into deformed metavolcanic rocks and formed hematite, epidote, titanite and green biotite in the granitoids (Witt & Davy in prep.; Libby et al. 1990). The particularly strong carbonation of mafic and ultramafic rocks in regional shear zones suggests a deep source for the CO_2-bearing fluids (Perring et al. 1990), but the ultimate source of these fluids is controversial (Burrows et al. 1986; Groves & Phillips 1987; Cameron 1988; reviewed by Kerrich 1990, and Perring et al. 1990).

Inclusions containing only CO_2 have been observed in some Archaean gold deposits (e.g. Robert & Kelly 1987), but these observations are at odds with thermodynamic calculations, which predict that significant amounts of water should also be present if the carbonic phase coexisted with an aqueous CO_2–H_2O fluid (e.g. Hall & Bodnar 1990). Kreulen (1987) has demonstrated that, in many cases, a significant volume of water (20–40 mole %) may remain undetected. Phase separation of an originally homogeneous fluid at the temperatures recorded by alteration assemblages at Sand King and Missouri (~500°C) could only occur with the addition of 10–12 wt % NaCl (Takenouchi & Kennedy 1964), much higher than the salinities of Type IV inclusions indicated by Raman microprobe analyses. Alternatively, strain-induced leakage of H_2O from inclusions (Hollister 1990; Bakker & Jansen 1990) may have led to CO_2 enrichment after entrapment. The latter process could account for the observed variations in the density of CO_2 in different inclusions, even within a single microfracture.

Mixed CO_2–CH_4–H_2O±NaCl fluids

At low fluid/rock ratios there would be redox exchange with iron in the upper crustal rocks, which may reduce the fO_2 of the fluid and convert some of the CO_2 to CH_4 via reactions such as:

$$6\,Fe_2SiO_4 + 7\,H_2O = 3\,Fe_3Si_2O_5(OH)_4 + Fe_3O_4 + H_2 \quad (1)$$

fayalite fluid serpentine magnetite

$$CO_2 + 4\,H_2 = CH_4 + 2\,H_2O \quad (2)$$

However, these reactions do not necessarily require a high hydrogen fugacity (Frost 1985) and this process is unlikely to generate the high CH_4/CO_2 ratios observed in some Type II and III inclusions. Therefore, other

processes such as fluid mixing or post-entrapment modification must be invoked. Evidence of fluid mixing between the CH_4-rich and CO_2-rich end-member fluids is given in Figure 11(A), which shows inclusions trapped in a microfracture parallel to the plane of the section. Large vapour-rich inclusions, some of which contain a muscovite crystal, grade into smaller, liquid-rich inclusions. Bulk compositions derived by the methods outlined in Ramboz et al. (1985) for the numbered inclusions in Figure 11(A) are given in Table 2. Figure 11(B) shows that the inclusions in the lower left of Figure 11(A) are CO_2-rich, while those in the upper right contain only CH_4 in the vapour phase, with mixed CO_2/CH_4 compositions being recorded from intermediate inclusions.

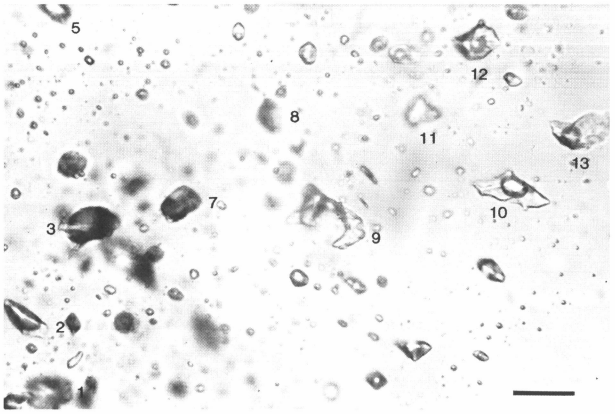

Figure 11(A). Photomicrograph of fluid inclusions in a single microfracture parallel to the plane of the page. There is a gradual progression from CO_2-rich, vapour-rich inclusions at the lower left to liquid-rich inclusions in the top right which contain only CH_4 in the vapour bubble, and this is interpreted as evidence for mixing between CO_2-rich and CH_4-bearing fluids. Analyses of the vapour phase of numbered inclusions are given in Table 2 (Nos 4, 6, and 14 are outside the field of view). Scale bar = 10μm.

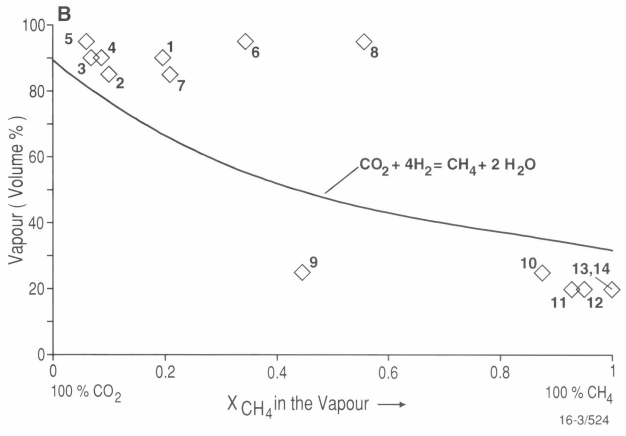

Figure 11(B). Plot of volume per cent vapour versus mole fraction of methane in the vapour bubble for the inclusions shown in Figure 11(A) and Table 2. The solid curve represents the predicted change in volume of the vapour bubble (assuming a constant vapour density) as a result of hydrogen diffusion into an inclusion initially containing 90 vol.% vapour. The CO_2 will be converted into CH_4 according to equation 2 (see text).

Addition of CH_4 to the CO_2–H_2O(±NaCl) system further expands the two-phase field to the conditions implied for mineralisation at Missouri and Sand King (cf. Duan et al. 1992). Phase separation of this complex fluid may have occurred over a range of pressures, owing to transient decreases in pressure, related to vein formation, yielding mixed CO_2+CH_4, vapour-rich inclusions and corresponding water-rich inclusions with varying vapour contents. Mixed CO_2+CH_4, vapour-rich inclusions are the most abundant Type III inclusions, but a few water-rich, Type III inclusions with a CO_2+CH_4 vapour phase have also been observed.

Table 2. Interpreted bulk composition derived from Raman microprobe analytical data for selected fluid inclusions from Figure 11.

Inclusion No.	*Vol. % vapor*	X_{CO_2}	X_{CH_4}	X_{H_2O}
1	90	0.667	0.158	0.175
2	85	0.623	0.073	0.304
3	90	0.762	0.063	0.175
4	90	0.737	0.070	0.193
5	95	0.853	0.039	0.108
6	95	0.597	0.299	0.104
7	85	0.588	0.155	0.257
8	95	0.403	0.503	0.094
9	25	0.023	0.021	0.956
10	25	0.003	0.017	0.970
11	20	0.001	0.022	0.977
12	20	0.001	0.022	0.977
13	20	0.000	0.017	0.983
14	20	0.000	0.017	0.983

Type II inclusions, on the other hand, display a more constant chemical composition than do Type III inclusions. They may represent the vapour-rich end-members generated by phase separation of an initially homogeneous CH_4–CO_2–H_2O fluid. Ubiquitous muscovite in these inclusions may have been soluble in this supercritical fluid or may have been accidentally trapped. Type II inclusions may also have been further modified by post-entrapment changes.

The aqueous fluids

The morphology of the low-salinity Type V inclusions indicates that they are relatively low-temperature, secondary inclusions. The low homogenisation temperatures (≤253°C) are in accord with the late influx of this fluid, which is possibly of meteoric origin. The saline fluids trapped by Type VI inclusions are similar to those observed by Robert & Kelly (1987) from the Sigma mine in the Abitibi Greenstone Belt, Canada. Calcium-dominated, saline formation waters are common in many sedimentary basins (e.g. Wilson & Long 1992), and are believed to originate from either diagenetic or modified connate brines (Land 1992). Overlapping homogenisation temperatures for Type V and Type VI inclusions (Fig. 10) suggest a broad contemporaneity between the two fluids. The higher homogenisation temperatures of some Type V inclusions may indicate their early entry into the still warm host rocks or, alternatively, may simply result from necking down. The higher Na^+ content of the saline fluid inclusions in calcite may reflect changes in the cation ratios which occurred as the Ca^{2+} ions were removed from the fluid under conditions favourable for the precipitation of carbonate minerals.

Fluid evolution

The textural evidence suggests that Type I inclusions were trapped in the early phases of mineralisation at both Sand King and Missouri. The Type I fluid inclusions indicate the presence of an initially low fO_2 fluid, which may have resulted from serpentinisation of the ultramafic units near these deposits. The widespread occurrence of native metals in many serpentinites indicates that they may form under conditions of extremely low fO_2 where the activity of hydrogen is relatively high. Frost (1985) has shown that, even under amphibolite-grade metamorphic conditions, there is a considerable gradient in fO_2 across a serpentinite body from a partially serpentinised core to a carbonatised margin. Oxygen fugacity progressively decreases towards the centre of the body until it reaches a minimum at the serpentinisation front, which may be up to four or five log units below the QFM buffer. Owing to the zone of strong reduction at the serpentinisation front, X_{CO_2} in this region will also fall and CO_2 will be converted to CH_4. The water-rich inclusions shown in Figure 11(A) are assumed to represent the end-member composition for Type I fluids. The calculated density of methane in these inclusions varies from 0.14 to 0.25 g.cm^{-3} and the average bulk density is estimated to be 0.78 g.cm^{-3}. Isochores calculated from the equation of state derived by Jacobs & Kerrick (1981) for CH_4–H_2O fluids with densities of 0.5–0.8 g.cm^{-3} are shown in Figure 12. Type IV inclusions contain only minor amounts of CH_4 and, although they show some evidence of necking or partial decrepitation, they do not appear to have been greatly affected by other post-entrapment changes or fluid mixing. Thus, they represent a CO_2–H_2O fluid which was generated or circulating after the system became more oxidised. The small amount of methane in the Type IV inclusions was taken into account by expressing the density of the carbonic phase in terms of 'equivalent CO_2' density and by using the data from Swanenberg (1979) and Heyen et al. (1982). This gives densities between 0.80 and 0.93 for Type IV inclusions, as shown by the 'equivalent CO_2'–H_2O isochores in Figure 12. The densities of CH_4-bearing and CO_2-bearing fluids are consistent with both having been trapped at the P–T conditions (450–600°C, 3–4 kbar) implied for the hydrothermal alteration and gold mineralisation.

The CO_2–H_2O fluids may have accompanied relatively oxidised I-type magmas during their ascent through the crust (Holloway 1976) and subsequent emplacement in the Siberia metavolcanic rocks. The CO_2-rich fluid appears to have been present before and during formation of the auriferous structures and gold-related metasomatism of the wallrocks. Thus, it seems most likely that the CH_4-rich fluid was locally generated in mafic or ultramafic units which may have been carbonated at their margins during interaction with the CO_2-rich fluid, but have retained a very low fO_2 at the serpentinisation front (Frost 1985), as described above.

The presence of muscovite and carbonate in Types II and III also provides a link with the potassic alteration event associated with gold mineralisation in both deposits. As shown in Figure 5, Type III inclusions exhibit a wide range of compositions and degree of fill. These variations may be the result of mixing between CO_2-rich and CH_4-rich fluids, as evident in Figure 11. The higher salinity of Type II inclusions (Fig. 7) suggests that they may be linked to the intrusion of the granitic magma. Additionally, Type II and some Type III inclusions may represent the products of phase separation from a mixed

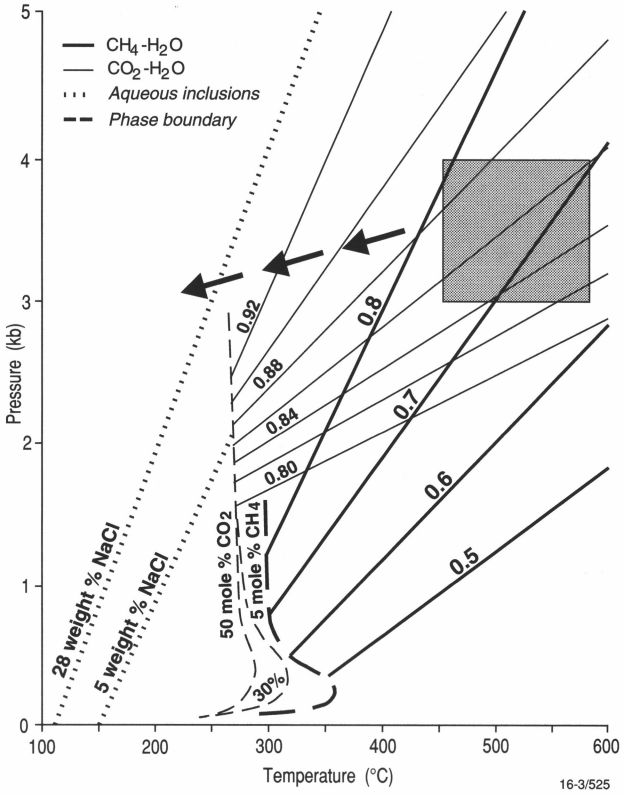

Figure 12. P–T diagram showing selected isochores representing the range of inclusions encountered at the Missouri and Sand King deposits. CH_4–H_2O (Type I) isochores are shown as thick lines, CO_2–H_2O (Type IV) as thin lines, and aqueous solutions containing 5 wt% NaCl (Type V) and 28 wt% NaCl (Type VI), respectively, as dotted lines. The mixed CH_4–CO_2–H_2O isochores for Types II and III have been omitted for clarity, but Duan et al. (1992) have shown that these are generally steeper than the corresponding CO_2–H_2O isochores. The numbers on the isochores represent fluid densities in g.cm^{-3}. Isoplethic phase boundary curves for H_2O systems with 5 mole % CH_4, 30 mole % CO_2 and 50 mole % CO_2 are also shown. The shaded region represents the approximate P–T conditions of gold deposition and potassic alteration as indicated by alteration assemblages and other geological relationships, and the arrows indicate a possible, close to isobaric, cooling path.

CO_2–CH_4–H_2O fluid. The range of CO_2/CH_4 ratios and liquid/vapour ratios defined by Type II and III inclusions could be generated if a compositionally variable, mixed CO_2–CH_4–H_2O fluid underwent phase separation over a range of transient pressures related to vein formation. However, necking-down and other post-entrapment changes (see below) may also have contributed to the range of vapour contents and CO_2/CH_4 ratios.

The P–T path during the latter stages of cooling is unknown, but is likely to have been essentially isobaric. Figure 12 indicates that the influx of low-salinity fluids, possibly of meteoric origin, was the next event, followed by the late influx of saline, $CaCl_2$-bearing brines.

The effect of post-entrapment changes to fluid inclusions

Recently, Hall et al. (1991) examined the evidence for hydrogen mobility at amphibolite to granulite facies conditions and have provided evidence for diffusion of

hydrogen into peak metamorphic fluid inclusions. This has been verified experimentally by Morgan et al. (1993), who re-equilibrated CO_2-rich inclusions in quartz and olivine at controlled fH_2 conditions at 718–728°C and 2 kbar. The experiments on isolated inclusions in quartz produced binary CO_2 (47–63 mol. %)–CH_4 (37–53 mol. %) gas mixtures, and even higher CH_4 contents were noted along secondary trails. The diffusion of H_2 into CO_2-rich inclusions leads to the formation of methane and water via reaction (2). The effect of this reaction on an inclusion which initially contains 90 vol. % CO_2 vapour is shown by the line in Figure 11(B). Although this line may be displaced either up or down, according to the initial vapour content of the inclusion, it is clear that, in all cases, most inclusions in Figure 11(B) do not plot close to this line. Therefore, hydrogen diffusion has not had a significant effect on these inclusions, and fluid mixing is thus the major mechanism controlling the compositional variation in Types II and III inclusions at Missouri and Sand King.

Inclusions which contain mixtures of CO_2 and CH_4 are also expected to precipitate graphite by the following reaction:

$$CO_2 + CH_4 = 2H_2O + 2C \qquad (3)$$

However, graphite was not detected with the Raman microprobe in any of the fluid inclusions examined in this study. The nucleation of graphite from fluids is known to involve a high activation energy (Ziegenbein & Johannes 1980) and will also be affected by slower nucleation kinetics and metastability at lower temperatures. Ramboz et al. (1985) suggested that CH_4-rich fluids may be produced at temperatures below the blocking temperature (approximately 370°C for the H_2O–CO_2–CH_4–graphite system). Furthermore, Morgan et al. (1993) noted that all their re-equilibration experiments in quartz resulted in a decrease in the pressure of the carbonic fluids and they calculated that the minimum density required for the stable formation of graphite is near 0.74 $g.cm^{-3}$. Therefore, the lower density of Types II and III inclusions from Sand King and Missouri may explain the absence of graphite in these inclusions.

The mechanisms for gold deposition

Low-salinity, H_2O–CO_2 fluids have been implicated as the ore-bearing fluid in many of the world's Archaean greenstone belts (Colvine et al. 1988; Roberts 1989; Ho et al. 1990), including the Eastern Goldfields Province, and it is probable that Type IV inclusion fluids had an important role in ore genesis at Missouri and Sand King. Methane is less ubiquitous in Archaean lode gold deposits, but its presence at Missouri and Sand King, as well as in many other deposits in the Eastern Goldfields (Ho et al. 1990; Mernagh & Witt 1993; Hagemann & Ridley 1993), has important implications for depositional models, especially where chemical reaction between hydrothermal fluids and Fe-rich host rocks (Groves & Phillips 1987) is not an appropriate mechanism.

The mixing of CO_2-rich and CH_4-rich fluids may result in large changes in the oxidation potential of the ore-bearing fluid. Figure 13 shows the major sulphur species expected at conditions similar to those of mineralisation at Missouri and Sand King. A high total-sulphur concentration has been adopted in accord with the suggestion by Mikucki & Ridley (1993) that fluids in amphibolite facies deposits may contain from 1–10 molal total sulphur.

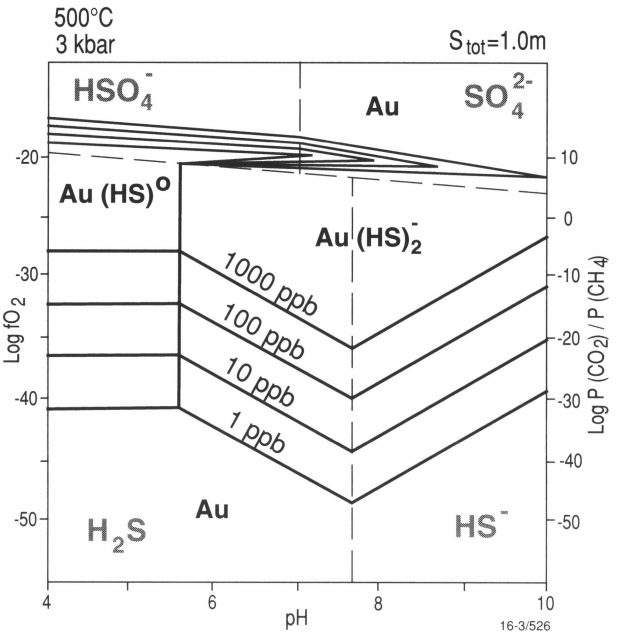

Figure 13. Log fO_2 versus pH diagram, showing solubility contours for the gold thio-complexes (ΣS = 1.0m) at 500°C and 3 kbar. Note that the stabilities of the thio-complexes have been extrapolated from the data of Hayashi & Ohmoto (1991), and remain speculative until they are experimentally verified. The corresponding CO_2/CH_4 ratios under the same conditions are shown on the right ordinate.

Note that Figure 13 is highly speculative, and was produced by extrapolating the data of Hayashi & Ohmoto (1991), which was obtained at or below 350°C. Nevertheless, it does show clearly that gold is probably transported either as the $Au(HS)^0$ or $Au(HS)_2^-$ complex under these conditions, and that relatively high concentrations of gold may be transported in methane-dominated fluids or fluids near the CO_2/CH_4 buffer. Gold will be precipitated as the fluid is oxidised and CO_2 becomes the dominant gaseous species.

However, the consequences of fluid mixing in these amphibolite-grade, lode-gold deposits should not be overlooked, as even minor increases in the CH_4 concentration of the ore-bearing fluid will greatly increase the immiscibility field in the CO_2–CH_4–H_2O–NaCl system. Duan et al. (1992) have shown that even the addition of a few mole per cent of CH_4 to the CO_2–H_2O system greatly increases the field of immiscibility and generally steepens the corresponding isochores. Addition of NaCl to the CO_2–H_2O system also increases the two-phase field (Bowers & Helgeson 1983), and Krader & Frank (1987) have shown that this effect is even greater in the CH_4–H_2O–NaCl system. In the latter case, the addition of 8 wt % NaCl extended the two-phase field from just over 300°C up to 500°C.

Hydrogen sulphide will be strongly partitioned into the (CH_4+CO_2)-rich vapour phase during phase separation, and gold will be deposited as a direct consequence of destabilisation of the aqueous auriferous sulphide complexes. Thus, the loss of sulphur as H_2S during phase separation and the resulting decrease in a_{H_2S} are important factors which may control gold precipitation under greenschist and amphibolite facies conditions. Fluids which contain methane will unmix over a wider range of

pressures and temperatures than for the corresponding CO_2–H_2O system and, thus, would enable this mechanism to operate to considerable depths within the crust.

Conclusions

From the distribution of fluid inclusions in quartz and carbonate from the Sand King and Missouri deposits and microthermometric and Raman microprobe data, we conclude that the earliest fluid (Type I) was trapped at a temperature of 500–600°C and a pressure of at least 3 kbar.

At approximately the same time as peak metamorphism and the intrusion of the nearby syn-D_3 granitoids there was an influx of CO_2-rich fluid. Mixing of this fluid with a CH_4–H_2O fluid from a possible ultramafic source and heterogeneous entrapment generated inclusions with a wide range of densities and CO_2/CH_4 ratios. The muscovite crystals observed in a number of Type II and Type III inclusions indicate a link between these fluids and the potassic alteration event evident in both deposits. The presence of CO_2-rich (Type IV) inclusions unaffected by the above processes suggests that CO_2-rich fluids continued to circulate after consumption of the CH_4-bearing fluid and the decrease in the activity of H_2 in the system. These events were followed by the influx of a low-salinity (meteoric?) fluid and, later, by a $CaCl_2$-rich (connate?) brine.

The prevalence of CO_2-bearing fluids in gold deposits in Archaean greenstone belts throughout the world suggests that mineralisation was associated with the influx of the CO_2-rich fluids. Methane enrichment of these fluids greatly increases the P–T range of fluid immiscibility, and H_2S, CH_4 and CO_2 would all be strongly partitioned into the vapour phase during unmixing of the ore fluid, leading to a decrease in the sulphur content of the residual fluid and, ultimately, gold precipitation. These mechanisms may operate over a wider range of pressures and temperatures than for the corresponding CO_2–H_2O system, thus enabling gold precipitation to occur at considerable depths within the crust.

Acknowledgments

We wish to thank Kalgoorlie Gold Operations for access to samples from Sand King and Missouri, and Christoph Heinrich, Greg Ewers and Brian Oversby for helpful discussions and comments. Thanks also to the referees, Robert Kerrich, Phillip Brown and Kenneth McQueen, for constructive reviews which helped improve this manuscript. W.K.W. publishes with permission of the Director of the Geological Survey of Western Australia.

References

Arculus, R.J. & Delano, J.W., 1981. Intrinsic oxygen fugacity measurements: techniques and results for spinels from upper mantle peridotite and megacryst assemblages. *Geochimica et Cosmochimica Acta*, 45, 899–913.

Arculus, R.J., Dawson, J.B., Mitchell, R.H., Gust, D.A. & Holmes, R.D., 1984. Oxidation states of the upper mantle recorded by megacryst ilmenite in kimberlite and type A and B spinel lherzolites. *Contributions to Mineralogy and Petrology*, 85, 85–94.

Bakker, R.J. & Jansen, B.H., 1990. Preferential water leakage from fluid inclusions by means of mobile dislocations. *Nature*, 345, 58–60.

Bird, P. & Pilapil, L., 1988. Description of mining operations at Sand King and Theil Well, Siberia. Unpublished report, Western Mining Corporation.

Bowers, T.S. & Helgeson, H.C., 1983. Calculation of the thermodynamic and geochemical consequences of nonideal mixing in the system H_2O–CO_2–NaCl on phase relations in geologic systems: Equation of state for H_2O–CO_2–NaCl fluids at high pressures and temperatures. *Geochimica et Cosmochimica Acta*, 47, 1247–1275.

Buddington, A.F. & Lindsley, D.H., 1964. Iron-titanium oxide minerals and synthetic equivalents. *Journal of Petrology*, 5, 310–357.

Burrows, D.R., Wood, P.C. & Spooner, E.T.C., 1986. Carbon isotope evidence for a magmatic origin for Archaean gold-quartz vein ore deposits. *Nature*, 321, 851–854.

Cameron, E.M., 1988. Archaean gold: relation to granulite formation and redox zoning in the crust. *Geology*, 16, 109–112.

Colvine, A.C., Fyon, J.A., Heather, K.B., Marmont, S., Smith, P.M. & Troop, D.G., 1988. Archaean lode gold deposits in Ontario. *Ontario Geological Survey Miscellaneous Paper*, 139.

Crawford, M.L., 1981. Phase equilibria in aqueous fluid inclusions. In Hollister, L.S. & Crawford, M.L. (editors). *Fluid inclusions, applications to petrology.* Mineralogical Association of Canada, 75–100.

Davis, D.W., Lowenstein, T.K. & Spencer, R.J., 1990. Melting behaviour of fluid inclusions in laboratory-grown halite crystals in the systems NaCl–H_2O, NaCl–KCl–H_2O, NaCl–$MgCl_2$–H_2O, and NaCl–$CaCl_2$–H_2O. *Geochimica et Cosmochimica Acta*, 54, 591–601.

Donnelly, H.G. & Katz, D.L., 1954. Phase equilibrium in the carbon-dioxide–methane system. *Industrial Engineering Chemistry*, 46, 511–517.

Duan, Z., Møller, N. & Weare, J.H., 1992. An equation of state for the CH_4–CO_2–H_2O system: II. mixtures from 50 to 1000°C and 0 to 1000 bar. *Geochimica et Cosmochimica Acta*, 56, 2619–2631.

Dubessy, J., Poty, B. & Ramboz, C., 1989. Advances in C–O–H–N–S fluid geochemistry based on micro-Raman spectrometric analysis of fluid inclusions. *European Journal of Mineralogy*, 1, 517–534.

Eggler, D.H., 1983. Upper mantle oxidation state: evidence from olivine–orthopyroxene–ilmenite assemblages. *Geophysical Research Letters*, 10, 365–368.

Frost, B.R., 1985. On the stability of sulfides, oxides, and native metals in serpentinite. *Journal of Petrology*, 26, 31–63.

Foster, R.P., 1989. Archaean gold mineralization in Zimbabwe: implications for metallogenesis and exploration. *In* Keays, R.R., Ramsay, W.R.H. & Groves, D.I. (editors). The geology of gold deposits: the perspective in 1988. *Economic Geology Monograph*, 6, 54–70.

Groves, D.I., 1993. An integrated model for genesis of Archaean gold mineralisation within the Yilgarn Block, Western Australia. *In* Williams, P.R. & Haldane, J.A. (compilers). An international conference on crustal evolution, metallogeny and exploration of the Eastern Goldfields, Extended Abstracts, *Australian Geological Survey Organisation, Record,* 1993/54, 115–121.

Groves, D.I., Barley, M.E., Barnicoat, A.C., Cassidy, K.F., Fare, R.J., Hagemann, S.G., Ho, S.E., Hronsky, J.M.A., Mikucki, E.J., Mueller, A.G., McNaughton, N.J., Perring, C.S., Ridley, J.R. & Vearncombe, J.R., 1992. Sub-greenschist to granulite-hosted Archaean lode-gold deposits of the Yilgarn Craton: a depositional contin-

uum from deep-sourced hydrothermal fluids in crustal-scale plumbing systems. *Geology Department (Key Centre) & University Extension, The University of Western Australia Publication*, 22, 325–337.

Groves, D.I. & Phillips, G.N., 1987. The genesis and tectonic controls on Archaean gold deposits of the Western Australian Shield: a metamorphic replacement model. *Ore Geology Reviews*, 2, 287–322.

Hagemann, S.G., Groves, D.I., Ridley, J.R. & Vearncombe, J.R., 1992. The Archaean lode-gold deposits at Wiluna, Western Australia: high level brittle-style mineralisation in a strike-slip regime. *Economic Geology*, 87, 1022–1053.

Hagemann, S.G. & Ridley, J.R., 1993. Hydrothermal fluids in epi- and katazonal crustal levels in the Archaean: implications for P–T–X–t evolution of lode-gold mineralisation. *In* Williams, P.R. & Haldane, J.A. (compilers). An international conference on crustal evolution, metallogeny and exploration of the Eastern Goldfields, Extended Abstracts, *Australian Geological Survey Organisation, Record*, 1993/54, 123–130.

Haggerty, S.E. & Tompkins, L.A., 1985. The redox state of the Earth's upper mantle from kimberlitic ilmenites. *Nature*, 303, 295–300.

Hall, D.L. & Bodnar, R.J., 1990. Methane in fluid inclusions from granulites: a product of hydrogen diffusion. *Geochimica et Cosmochimica Acta*, 54, 641–651.

Hall, D.L., Bodnar, R.J. & Craig, J.R., 1991. Evidence for postentrapment diffusion of hydrogen into peak metamorphic fluid inclusions from the massive sulfide deposits at Ducktown, Tennessee. *American Mineralogist*, 76, 1344–1355.

Hayashi, K. & Ohmoto, H., 1991. Solubility of gold in NaCl- and H_2S-bearing aqueous solutions at 250–350°C. *Geochimica et Cosmochimica Acta*, 55, 2111–2126.

Heyen, G., Ramboz, C. & Dubessy, J., 1982. Simulation des equilibres de phases dans le system CO_2–CH_4 en dessous de 50°C et de 100 bar. Application aux inclusions fluides. *Comptes rendus de Academie des Sciences, Paris*, 294, Serie II, 203–206.

Hill, B.D. & Bird, P., 1990. Sand King gold deposit. *In* Hughes, F.E. (editor). *Geology of the mineral deposits of Australia and Papua New Guinea.* The Australasian Institute of Mining and Metallurgy, Melbourne, 377–381.

Ho, S.E., Bennett, J.M., Cassidy, K.F., Hronsky, J.M.A., Mikucki, E.J. & Sang, J.H., 1990. Nature of ore fluid, and transportational and depositional conditions in sub-amphibolite facies deposits. In Ho, S.E., Groves, D.I. & Bennett, J.M., (editors). Gold deposits of the Archaean Yilgarn block, Western Australia: nature, genesis and exploration guides. *The University of Western Australia, Geology Department and University Extension, Publication,* 20, 198–211.

Hollister, L.S., 1990. Enrichment of CO_2 in fluid inclusions in quartz by removal of H_2O during crystal-plastic deformation. *Journal of Structural Geology*, 12, 895–901.

Hollister, L.S. & Burrus, R.C., 1976. Phase equilibria in fluid inclusions from the Khtada Lake metamorphic complex. *Geochimica et Cosmochimica Acta*, 40, 163–175.

Holloway, J.R., 1976. Fluids in the evolution of granitic magmas: Consequences of finite CO_2 solubility. *Geological Society of America Bulletin*, 87, 1513-1518.

Holloway, J.R., 1981. Compositions and volumes of supercritical fluids in the Earth's crust. *In* Hollister, L.S., & Crawford, M.L. (editors). *Fluid inclusions: applications to petrology*. Mineralogical Association of Canada, 13–38.

Holloway, J.R., 1984. Graphite–CH_4–H_2O–CO_2 equilibria at low-grade metamorphic conditions. *Geology*, 12, 455–458.

Jacobs, G.K. & Kerrick, D.M., 1981. Methane: an equation of state with application to the ternary system H_2O–CO_2–CH_4. *Geochimica et Cosmochimica Acta*, 45, 607–614.

Kerrich, R., 1990. Carbon-isotope systematics of Archaean Au–Ag vein deposits in the Superior Province: *Canadian Journal of Earth Sciences*, 27, 40–56.

Konnerup-Madsen J., Dubessy, J. & Rose-Hansen, J., 1985. Combined Raman microprobe spectrometry and microthermometry of fluid inclusions in minerals from igneous rocks of the Gardar province (south Greenland). *Lithos*, 18, 271–280.

Krader, T. & Franck, E.U., 1987. The ternary systems H_2O–CH_4–NaCl and H_2O–CH_4–$CaCl_2$ to 800K and 250 MPa. *Berichte der Bunsengesellschaft fuer Physikalische Chemie*, 91, 627–634.

Kreulen, R., 1987. Thermodynamic calculations of the C–O–H system applied to fluid inclusions: are fluid inclusions unbiased samples of ancient fluids? *Chemical Geology*, 61, 59–64.

Land, L.S., 1992. Saline formation waters in sedimentary basins: connate or diagenetic? *In* Kharaka, Y. & Maest, A.S., (editors). *Water–rock interaction.* Balkema, Rotterdam, 865–868.

Lapointe, B. & Chown, E.H., 1993. Gold-bearing iron-formation in a granulite terrane of the Canadian Shield: a possible deep-level expression of an Archean gold-mineralizing system, *Mineralium Deposita*, 28, 191–197.

Larsen, R.B., Brooks, C.K. & Bird, D.K., 1992. Methane-bearing, aqueous, saline solutions in the Skaergaard intrusion, east Greenland. *Contributions to Mineralogy and Petrology*, 112, 428–437.

Libby, J.W., Barley, M.E., Eisenlohr, B.N., Groves, D.I., Hronsky, J.M.A., Vearncombe, J.R., 1990. Structural setting of gold deposits: craton-scale deformation zones. *In* Ho, S.E., Groves, D.I. & Bennett, J.M., (editors). Gold deposits of the Archaean Yilgarn block, Western Australia: nature, genesis and exploration guides. *University of Western Australia, Geology Department and University Extension, Publication,* 20, 30–37.

Liu, L. & Mernagh, T.P., 1990. Phase transitions and Raman spectra of calcite at high pressures and room temperature. *American Mineralogist*, 75, 801–806.

Mattioli, G.S. & Wood, B.J., 1986. Upper mantle oxygen fugacity recorded by spinel lherzolites, *Nature*, 322, 626–628.

McNaughton, N.J., Groves, D.I. & Witt, W.K., 1993. The source of lead in Archaean lode gold deposits of the Menzies–Kalgoorlie–Kambalda region, Yilgarn Block, Western Australia, *Mineralium Deposita*, 28, 495–502.

Mernagh, T.P. & Wilde, A.R., 1989. The use of the laser Raman microprobe for the determination of salinity in fluid inclusions. *Geochimica et Cosmochimica Acta*, 53, 765–771.

Mernagh, T.P. & Witt, W.K., 1993. The relationship between gold mineralisation and metamorphic grade in the Menzies–Kambalda area, Eastern Goldfields, W.A.: evidence from fluid inclusions. *Australian Geological Survey Organisation, Record*, 1993/27.

Mikucki, E.J. & Ridley, J.R., 1993. The hydrothermal fluid of Archaean lode-gold deposits at different

metamorphic grades: compositional constraints from ore and wallrock alteration assemblages. *Mineralium Deposita*, 28, 469–481.

Montgomery, A., 1909. Report on the Waverly or Siberia District, Western Australia. *Department of Mines Western Australia, Annual Report.*

Morgan, G.B., Chou, I-M., Pasteris, J.D. & Olsen, S.N., 1993. Re-equilibration of CO_2 fluid inclusions at controlled hydrogen fugacities. *Journal of Metamorphic Geology*, 11, 155–164.

Myers, J.S., 1990. *In* Geology and Mineral Resources of Western Australia. *Western Australia Geological Survey, Memoir* 3, 126–127.

Ohmoto, H. & Kerrick, D., 1977. Devolatilization equilibria in graphitic systems. American Journal of Science, 277, 1013–1044.

Pasteris, J.D., Wopenka, B. & Seitz, J.C., 1988. Practical aspects of quantitative laser Raman microprobe spectroscopy for the study of fluid inclusions. Geochimica et Cosmochimica Acta, 52, 979–988.

Perring, C.S., Barley, M.E., Groves, D.I., McNaughton, N.J. & Ridley, J.R., 1990. Fluid and metal sources. *In* Ho, S.E., Groves, D.I. & Bennett, J.M., (editors). Gold deposits of the Archaean Yilgarn block, Western Australia: nature, genesis and exploration guides. *University of Western Australia, Geology Department and University Extension, Publication,* 20, 285–291.

Poutiainen, M., 1990. Evolution of a metamorphic fluid during progressive metamorphism in the Joroinen-Sulkava area, southeastern Finland, as indicated by fluid inclusions. *Mineralogical Magazine*, 54, 207–218.

Ramboz, C., Schnapper, D. & Dubessy, J., 1985. The P–V–T–X–fO_2 evolution of H_2O–CO_2–CH_4-bearing fluid in a wolframite vein: reconstruction from fluid inclusion studies. *Geochimica et Cosmochimica Acta*, 49, 205–219.

Robert, F. & Brown, A.C., 1986. Archean gold-bearing quartz veins at the Sigma mine, Abitibi greenstone belt, Quebec. Part I. Geologic relations and formation of the vein systems. Economic Geology, 81, 578–592.

Robert, F. & Kelly, W.C., 1987. Ore-forming fluids in Archean gold-bearing quartz veins at the Sigma mine, Abitibi greenstone belt, Quebec, Canada. *Economic Geology*, 82, 1464–1482.

Roberts, R.G., 1989. Archean lode gold deposits. In Roberts, R.G. & Sheahan, P.A. (editors). Ore Deposit Models, *Geoscience Canada, Reprint Series*, 3, 1–19.

Rumble, D., III & Hoering, T.C., 1986. Carbon isotope geochemistry of graphite vein deposits from New Hampshire, U.S.A. *Geochimica et Cosmochimica Acta*, 50, 1239–1247.

Santosh, M., Jackson, D.H., Harris, N.B.W. & Mattey, D.P., 1991. Carbonic fluid inclusions in South Indian granulites: evidence for entrapment during charnockite formation. *Contributions to Mineralogy and Petrology*, 108, 318–330.

Seitz, J.C., Pasteris, J.D. & Wopenka, B., 1987. Characterization of CO_2–CH_4–H_2O fluid inclusions by microthermometry and laser Raman microprobe spectroscopy: inferences for clathrate and fluid equilibria. *Geochimica et Cosmochimica Acta*, 51, 1651–1664.

Shepherd, T.J., Rankin, S.H. & Alderton, D.H.M., 1985. *A practical guide to fluid inclusion studies*. Blackie, London, 235 pp.

Smith, B.H., 1983. Siberia and Ora Banda laterites. *In* Smith, B.H., (Editor). *Geochemical exploration in the Eastern Goldfields region of Western Australia, Tour Guide.* The Association of Exploration Geochemists.

Smith, T.J., Cloke, P.L. & Kesler, S.E., 1984. Geochemistry of fluid inclusions from the McIntyre–Hollinger gold deposit, Timmins, Ontario, Canada. *Economic Geology*, 79, 1265–1285.

Swanenberg, H.E.C., 1979. Phase equilibria in carbonic systems, and their application to freezing studies of fluid inclusions. *Contributions to Mineralogy and Petrology*, 68, 303–306.

Takenouchi, S. & Kennedy, G.C., 1964. The binary system H_2O–CO_2 at high temperatures and pressures. *American Journal of Science*, 262, 1055–1074.

Thomas, A.V., Pasteris, J.D., Bray, C.J. & Spooner, E.T.C., 1990. H_2O–CH_4–NaCl–CO_2 inclusions from the footwall contact of the Tanco granitic pegmatite: estimates of internal pressure and composition from microthermometry, laser Raman spectroscopy, and gas chromatography. *Geochimica et Cosmochimica Acta*, 54, 559–573.

Walshe, J.L., 1986. A six-component chlorite solid solution model and the conditions of chlorite formation in hydrothermal and geothermal systems. *Economic Geology*, 81, 681–703.

Wilkins, R.W.T. & Barkas, J.P., 1978. Fluid inclusions, deformation and recrystallization in granite tectonites. *Contributions to Mineralogy and Petrology*, 65, 293–299.

Wilson, T.P. & Long, D.T., 1992. Evolution of $CaCl_2$ brine in Silurian aged formations of the Michigan basin, USA: the role of mineralogic reactions and evaporite diagenesis. *In* Kharaka, Y. & Maest, A.S., (editors). *Water-rock interaction*. Balkema, Rotterdam, 1213–1216.

Witt, W.K., 1991. Regional metamorphic controls on alteration associated with gold mineralization in the Eastern Goldfields province, Western Australia: implications for the timing and origin of Archean lode-gold deposits. *Geology*, 19, 982–985.

Witt, W.K., 1992. Porphyry intrusions and albitites in the Bardoc–Kalgoorlie area, Western Australia, and their role in Archean epigenetic gold mineralization. *Canadian Journal of Earth Sciences*, 29, 1609–1622.

Witt, W.K., 1993a. Lithological and structural controls on gold mineralization in the Archaean Menzies–Kambalda area, Western Australia. *Australian Journal of Earth Sciences*, 40, 65–86.

Witt, W.K., 1993b. Gold deposits of the Mount Pleasant Ora Banda areas, Western Australia—Part 1 of a systematic study of the gold mines in the Menzies–Kambalda region, Western Australia. *Western Australia Geological Survey, Record*, 1992/14, 104 pp.

Witt, W.K. & Davy, R., in prep. Granitoids of the southwest Eastern Goldfields Province, W.A. *Western Australian Geological Survey, Report.*

Woods, T.L., Bethke, P.M., Bodnar, R.J. & Werre, R.W., 1981. Supplementary components and operation of the U.S. Geological Survey gas-flow heating/freezing stage. *U.S. Geological Survey Open-file Report*, 81–954, 12 pp.

Wyche, S. & Witt, W.K., 1992. Geology of the Davyhurst 1:100 000 sheet, Western Australia. *Western Australia Geological Survey, Record* 1991/3, 48 pp.

Ziegenbeim, D. & Johannes, W., 1980. Graphite in C–H–O fluids: an unsuitable compound to buffer fluid composition at temperatures up to 700°C. *Neues Jahrbuch für Mineralogie: Abhandlungen*, 7, 289–305.